Dynamics of Pb(II) adsorption on nanostructured γ-alumina: calculations of axial dispersion and overall mass transfer coefficients in the fixed-bed column

Zahra Saadi, Reyhaneh Saadi and Reza Fazaeli

ABSTRACT

In the present study, the removal of metal ions Pb(II) using nanostructured γ-alumina was investigated by tests on batch operations and fixed-bed columns. Optimization was determined for factors effective on adsorption such as pH, contact time of metal solution with adsorbent and initial solution concentration. The optimum pH level was determined at 4.5 and the maximum adsorption percentage was achieved at 150 minutes. pH_{pzc} was measured 8.3 for nanostructured γ-Al_2O_3. The Langmuir, Freundlich and Temkin isotherms were used to analyze the experimental data. The Langmuir isotherm model showed the best agreement with the experimental data. The model showed evaluations for maximum adsorption capacity of adsorbent at 119.04 mg/g and adsorbent bed performance for different flow rates, bed heights and influent concentrations were also investigated. The lumped method was used to solve the bed equations, to predict the breakthrough curve and model overall mass transfer coefficient ($K_{overall}$) and axial dispersion coefficient (D_z) parameters to make comparisons with experimental results.

Key words | breakthrough curve, dynamic modeling, fixed-bed, lead, nanostructured γ-alumina

Zahra Saadi
Reyhaneh Saadi
Reza Fazaeli (corresponding author)
Department of Chemical Engineering, Faculty of Engineering, South Tehran Branch,
Islamic Azad University,
Tehran,
Iran
E-mail: *r_fazaeli@azad.ac.ir*

INTRODUCTION

Industrial wastewater polluted with heavy metals has endangered human health and the environment. Lead is one of the most extensively found toxic metals in the environment. According to the United States Environmental Protection Agency (USEPA) standards, the maximum allowable concentration of lead in drinking water is estimated at 0.006 mg/L (Barakat 2011). The adsorption process has proved an economical method for the removal of heavy metals from an aqueous solution. However, other materials, such as activated carbon, silica, titanium dioxide, calcium carbonate, and alumina, have also been effective for removing heavy metals from wastewater (Kim & Chung 2002). In recent years, nanotechnology has appeared as one of the key technologies for water treatment and various nanomaterials have been applied to remove heavy metals from wastewater, for example, nanometal-oxides (Zhang *et al.* 2008), carbon nanotubes (Ahmedna *et al.* 2004) and nanozeolite composites (Ngomsik *et al.* 2005). The advantages of nanomaterials include properties such as high reactivity due to unsaturated surface atoms; good adsorption capacity; small size; high surface area and regular crystalline formation that determine high potential for application in water treatment. Properties of nanoparticles that give them a high rate of adsorption determine the materials as an excellent choice for application in adsorption processes (Bhatnagara *et al.* 2010; Samadi *et al.* 2010). Nano-alumina has several crystalline forms but the most commonly used is γ-alumina. Considering the surface area of γ-alumina in the range of 150–500 m^2/g and a pore radius in the range of 1.5–6 nm, the form of γ-alumina is anticipated to be more active than the α-alumina.γ-Al_2O_3 nanoparticle and as such is a promising material as an adsorbent due to its large specific surface area, high adsorption capacity, mechanical strength and low temperature modification (Zhang *et al.* 2008).

doi: 10.2166/wh.2015.271

Afkhami *et al.* (2010) studied the removal of the metal cations Pb(II), Cd(II), Cr(III), Co(II), Ni(II) and Mn(II) from water samples by nano-alumina modified with 2,4-dinitrophenylhydrazine. Optimal experimental conditions including pH, adsorbent dosage and contact time have been established. Sulaymon *et al.* (2009) studied the removal of Pb(II), Cu(II), Cr(III) and Co(II) onto granular-activated carbon in batch and fixed-bed adsorbers. The effects of flow rate, bed height and initial metal ion concentration on the breakthrough curves have been studied. The equilibrium isotherm data, the external mass transfer coefficient and pore diffusion coefficient were obtained from separate experiments in batch adsorber by fitting the experimental data with a film-pore diffusion model.

The purpose of this study was to test the removal of Pb^{2+} by nanostructured γ-alumina using a fixed bed with an upward flow. Evaluations for metal uptake and effect of pH on the adsorption percentage were determined by batch experiments and the resulting data were analyzed by Langmuir, Freundlich and Temkin isotherms. Parameters of influent flow rate; initial Pb^{2+}concentration and bed height were tested in the fixed-bed column.

MATERIALS AND METHOD

Materials

Nanostructured γ-alumina was prepared from Nano-Pars-Lima Company as adsorbent and lead nitrate was obtained from the Merck Company for application as the adsorbate. In this study, all materials were prepared with high purity in order to increase reliability and validity as follows: double-distilled water was used; dilute HNO_3 and NaOH were used to adjust pH.

An atomic absorption spectrophotometer with acetylene flame (PG 990) was used for the measurement of lead ions; a digital pH meter (Sartorius (PB-11)) was used for the pH measurement. An accurate gas temperature controller (THC100) was used for controlling the temperature of a close plexiglass cube. Flow rates were regulated using a peristaltic pump (Etatron DS, Italy) capable of adjusting flow rates in the mL/min range. Evaluations for specific surface area were determined by N_2 gas Brunauer–Emmett–Teller (BET) analysis using a BET N_2 physisorption apparatus (Micrometrics ASAP 2010) at 76.42 K.

Each experimental data (effluent concentration) determination by atomic absorption spectrophotometer was repeated two or three times and the average result was reported in all graphs. The range of standard deviation for all experimental effluent concentrations was between 0.06 and 0.15.

Batch studies

Batch experiments were carried out two or three times in different sets using 30–120 mg/L lead with an initial concentration of 170 mg/L in contact with 0.5 g of nanostructured γ-alumina at pH 4.5 for 150 minutes at room temperature, 25°C ± 1. All experiments were carried out in a close plexiglass cube equipped with a gas temperature controller. pH was adjusted to 4.5 using dilute HNO_3, and NaOH. After a time period under agitation, suspensions were centrifuged at 10,000 rpm for 15 minutes. The supernatants were then collected and analyzed to determine cation concentrations by atomic adsorption spectrophotometry. The removal percentage was calculated using Equation (1) (Afkhami *et al.* 2010; Rahmani *et al.* 2010):

$$R\% = \frac{C_o - C_e}{C_o} \times 100 \quad (1)$$

Batch equilibrium experiments to determine the optimum pH were performed at various pH levels (2.5–6.5) under the same conditions.

The pH_{pzc} (point of zero charge) of the adsorbent was measured by the following method: 0.5 g of adsorbent was added to 100 mL of 0.1 M NaCl solution where the initial solution pH was adjusted using aqueous HNO_3 or NaOH solution. The reason for using NaCl solution is to fix ionic strength. The solution was allowed to mix for 24 hours. After this time the pH of the solution was measured. If the initial pH of the solution is equal to the pH_{pzc} of the adsorbent, no change in the pH will be observed after adding adsorbent to the solution (Dastgheib & Rockstraw 2002). Equilibrium time was determined by testing the shaking time of samples from 25 to 200 minutes. Adsorbent dose and solution pH were fixed at 5 g/L and 4.5 g/L,

respectively. The equilibrium time was determined as 150 minutes. Regeneration studies were not carried out in the present research. The saturated adsorbent can be regenerated using chemical regeneration (Rahmani *et al.* 2010).

Column studies

A Pyrex column, 30 cm in height and 1 cm in diameter was used for upward flow. A schematic diagram of the experimental column is shown in Figure 1. The adsorption column was packed with spherical particles of nanostructured γ-alumina between two layers of glass wool. Investigation of the effect of flow rate on the behavior of the adsorbent column was tested at flow rates of 3, 6 and 9 mL/min with constant concentrations of 100 ppm and a constant bed height of 10 cm was used. Investigations of the effect of height on behavior of the adsorbent column applied heights of 5, 10 and 15 cm (equivalent with 3.53, 7.06 and 10.6 g) with constant concentrations of 100 ppm and constant flow rate of 6 mL/min; and investigations of the effect of initial concentration of lead ion on the behavior of the adsorbent column applied concentrations 65,100 and 150 ppm with constant bed height of 10 cm and constant flow rate of 6 mL/min. How to fill the column was based on the equation ($\rho_p = 4W/\pi d_b^2 L$) which shows a relationship between the mass of the adsorbent and the bed height in the constant diameter column. Effluent solution from the column was collected at specified time intervals and measurements were taken for the remaining lead concentration in the solution using an atomic absorption spectrophotometer. In all experiments, temperature and pH values were adjusted to 25°C ± 1 and 4.5°C, respectively. The maximum adsorption capacity of the adsorbent in the fixed-bed column was calculated using Equations (2) and (3) (Unuabonah *et al.* 2012):

$$q_{total} = \frac{Q}{1000}\int_0^{t_{total}} (C_o - C_t)\,dt \quad (2)$$

$$q_{max} = \frac{q_{total}}{W} \quad (3)$$

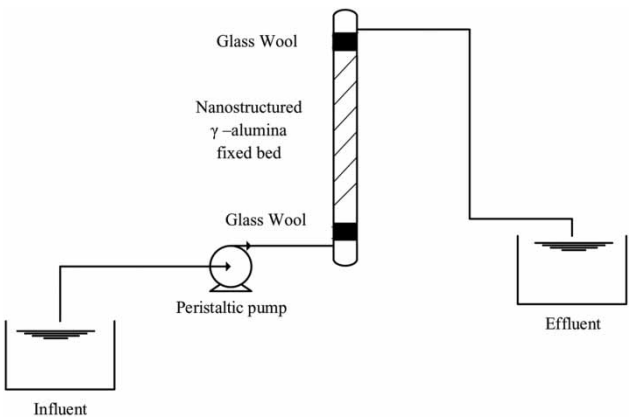

Figure 1 | Schematic diagram of the experimental column.

RESULTS AND DISCUSSION

Characterization of adsorbent

The spheres made from γ-alumina nano powder had an average size of 20 nm and were 2–3 mm in diameter. The BET surface area was about 138 m^2/g. The adsorbent particle density and porosity were 0.9 g/cm^3 and 0.52 g/cm^3, respectively. The chemical composition of the adsorbent was 99% Al_2O_3 (minimum), 25 ppm Ca (maximum), 7 ppm V (maximum), 315 ppm cl (maximum), 70 ppm Na (maximum), 3 ppm Mn (maximum) and 2 ppm Co (maximum). All these elements were present in their most stable oxide form.

Batch studies

Effect of pH

pH is one of the most important factors affecting the surface properties of an adsorbent and the surface charge of an adsorbent in an adsorption process (Sharma *et al.* 2010). A sample (0.5 g) of the adsorbent was solved in 100 mL solution of 30 mg/L metal ions at several pH values (2.5–6.5) in order to evaluate the influence of pH solution on Pb^{2+} adsorption. Samples were stirred by a magnetic stirrer at room temperature, 25°C ± 1 and after 150 minutes mixing samples were centrifuged and measurements were taken for the degree of adsorption using an atomic absorption spectrophotometer. The

pH_{pzc} of the nanostructured γ-alumina was measured at 8.3. If $pH_{solution} > pH_{pzc}$, negative surface charge of the adsorbent provides uptake of cations and at $pH_{solution} < pH_{pzc}$, the surface charge of the adsorbent is positive and the adsorbent can adsorb anions by electrostatic attraction. At a low pH (pH = 2), strong competition adsorption between protons and metal ions for the occupation of active sites and repulsion between the positive charge of the adsorbent surface and the Pb^{2+} limited the metal adsorption. However, in the range of pH between 2 and 4.5, these competition and repulsion effects decreased and metal ion adsorption increased. The maximum removal of metal ions (92.71%) and the maximum adsorption capacity (5.56 mg/g) were observed at pH 4.5 and the surface of the adsorbent was nearly covered with metal ions. At higher pH (pH > 4.5), competition adsorption between hydroxide ions and Pb^{2+} increased. Therefore, the adsorbent can adsorb hydroxide ions by electrostatic attraction and consequently, fewer metal ions are permitted to adsorb on the surface of the adsorbent. Due to the formation of lead hydroxide and its precipitation at neutralized and basic pH, the pH range was chosen as 2.5–6.5, i.e., formation of lead hydroxide at pH higher than 6.5 caused by the adsorption of Pb^{2+} species is negligible (Mobasherpour *et al.* 2011).

Effect of contact time

The time taken to reach the adsorbent equilibrium in adsorption systems design is important (Ho *et al.* 2005). All isotherm studies are based on the equilibrium concentration so that it is certain to reach equilibrium state. Equilibrium is achieved when changes in the equilibrium adsorption capacity of the adsorbent (q_e) are negligible. In order to determine the equilibrium time, a 0.5 g sample of the adsorbent was mixed in 100 mL 30 mg/L lead solution at various times (25–200 minutes) and at pH 4.5. After mixing and separating the solid phase from the liquid, lead concentrations were measured using an atomic absorption spectrophotometer. The removal efficiency increased to 150 minutes according to an increased contact time, but after 150 minutes removal efficiency remained constant. Consequently, the optimum contact time for Pb(II) adsorption was determined as 150 minutes and the maximum removal of metal ions and the maximum adsorption capacity at this time were 90.5% and 5.43 mg/g, respectively. The vacant sites at the initial times resulted in increased removal efficiency but under increased time the number of active sites decreased so there was increased competition for occupation of sites by the metal ions.

Adsorption isotherm

The uptake quantity for a range of concentrations of metal ions can be described by the adsorption isotherms that show how a solute interacts with a sorbent (Dabrowski 2001). In the present work, the Langmuir, Freundlich and Temkin isotherms were applied and the experimental results were compared with these models. The amount of metal ions adsorbed per unit mass of adsorbent is calculated by Equation (4):

$$q_e = \frac{V(C_o - C_e)}{W} \tag{4}$$

As determined in previous studies on the reaction mechanism, lead is predominantly chemisorbed onto the surface of the nanostructured γ-alumina (Iannibello & Marengo 1979; Cai & Sohlberg 2003).

Langmuir isotherm

According to the Langmuir assumptions, each adsorbent site can only adsorb one molecule or atom. In addition, adsorption is limited to one surface layer. The energy for adsorption is uniform and independent of surface coverage (Do 1998). The linear form of the Langmuir isotherm is given by Equation (5) (APHA 2005; Elouear *et al.* 2008):

$$\frac{1}{q_e} = \frac{1}{k_L q_{max}} \frac{1}{C_e} + \frac{1}{q_{max}} \tag{5}$$

k_L is related to the tendency of binding with adsorbent sites. Large values of k_L indicate a strong interaction between the metal and the adsorbent active sites. The Langmuir equation parameters, q_{max} and k_L, were obtained at 119.04 mg/g and 0.16 L/mg, respectively. These values were obtained from the slope and intercept of the linear plot of $1/q_e$ against $1/C_e$ (Figure 2) and are presented in Table 1. The most essential characteristics of the Langmuir

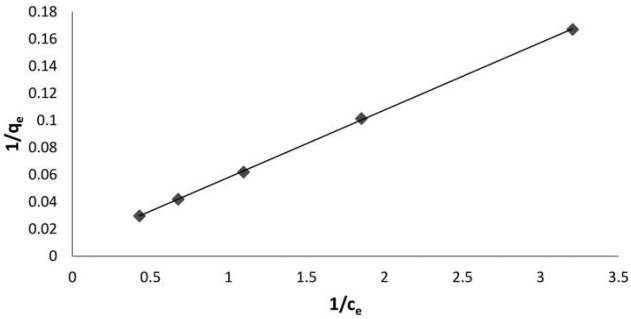

Figure 2 | Langmuir plot for adsorption of Pb(II) onto nanostructured γ-alumina. Conditions: adsorbent dose 5 g/L and pH 4.5.

Table 1 | Isotherm model constants

Isotherm	Parameter	Value
Langmuir	q_{max} (mg/g)	119.04
	k_L (L/mg)	0.16
	R^2	0.999
	MPSD	0.0003
	χ^2	0.003
Freundlich	*1/n*	0.86
	K_f ($mg^{1-n}L^ng^{-1}$)	16.76
	R^2	0.998
	MPSD	0.009
	χ^2	0.072
Temkin	B_T	13.68
	K_T	4.19
	R^2	0.96
	MPSD	0.191
	χ^2	2.099

isotherm can be expressed in terms of a dimensionless constant of separation factor or equilibrium parameter, R_L. Desirable or undesirable adsorption in the Langmuir equation can be calculated by this factor, as shown in Equation (6) (Afkhami *et al.* 2010):

$$R_L = \frac{1}{1 + k_L C_o} \tag{6}$$

$0 < R_L < 1$, $R_L = 0$ and $R_L = 1$ indicate favorable, irreversible and linear adsorption processes, respectively (Afkhami *et al.* 2010). An R_L of 0.16 was obtained, an evaluation that indicates favorable adsorption.

Freundlich isotherm

The Freundlich isotherm is an empirical isotherm, suitable for heterogeneous surfaces that follow the theory of Langmuir. Its general form is given in Equation (7) (Do 1998):

$$q_e = K_f C_e^{\frac{1}{n}} \tag{7}$$

The linear form of the Freundlich isotherm is given by Equation (8):

$$\log q_e = \log K_f = \frac{1}{n} \log C_e \tag{8}$$

K_f and n are Freundlich constants that indicate adsorption capacity and adsorption intensity, respectively. A plot of logarithmic curve q_e versus C_e (Figure 3) is a straight line with a slope of *1/n* and an intercept of log K_f. n and K_f values of 1.157 and 16.76 mg/g were obtained. These values are presented in Table 1. When $n = 1$, $n > 1$ and $n < 1$, this indicates linear equilibrium, favorable and unfavorable adsorption isotherms, respectively (Yang 1987). So, with reference to the values of n in this work, the adsorption process was favorable.

Temkin isotherm

The non-linear form of the Temkin isotherm is given by Equation (9) (Temkin & Pyzhev 1940):

$$q_e = B_T \ln(K_T C_e) \tag{9}$$

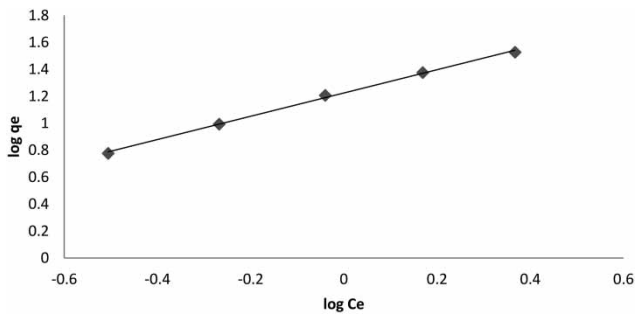

Figure 3 | Freundlich plot for adsorption of Pb(II) onto nanostructured γ-alumina. Conditions: adsorbent dose 5 g/L and pH 4.5.

The isotherm can be expressed in linear form as Equation (10):

$$q_e = B_T \ln K_T + B_T \ln C_e \quad (10)$$

B_T and K_T were determined as 13.68 and 4.19, respectively, from linear plot of *log* q_e versus *log* C_e (Figure 4). Temkin isotherm constants are given in Table 1. The correlation coefficient represents a good agreement between experimental data and the adsorption isotherm.

An error is required to evaluate the fit of an isotherm equation to the experimental equilibrium data obtained. In this study, two error functions, a derivative of Marquardt's Percent Standard Deviation (MPSD), (Ho *et al.* 2002) and chi-square analysis (χ^2) (Boulinguiez *et al.* 2008) were used to determine and evaluate the fit of the isotherm models to the experimental data. The MPSD and χ^2 error functions are expressed as Equations (11) and (12), respectively:

$$\sum_{i=1}^{P} \left(\frac{q_{exp} - q_{cal}}{q_{exp}} \right)_i^2 \quad (11)$$

$$x^2 = \sum_{i=1}^{n} \frac{(q_{exp} - q_{cal})^2}{q_{cal}} \quad (12)$$

The correlation coefficients (R^2) for the three isotherms Langmuir, Freundlich and Temkin were 0.999, 0.998 and 0.96, respectively.

If data from the model were similar to the experimental data, the error value would be a small number and vice versa. These results indicate that the Langmuir isotherm provided a better fit to the experimental data compared to the other isotherms because it had the highest R^2 and the least amount of errors.

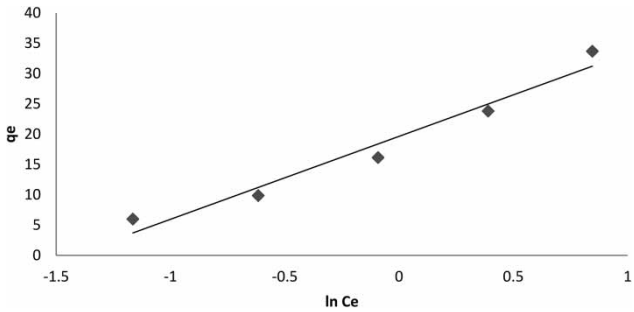

Figure 4 | Temkin plot of adsorption of Pb(II) onto nanostructured γ-alumina. Conditions: adsorbent dose 5 g/L and pH 4.5.

Column studies

Breakthrough studies

Appropriate and successful design of an adsorbent column requires an accurate prediction of the concentration-time profile or breakthrough curve for the outlet flow from the bed. This is also possible by modeling of the adsorption process. Since the maximum uptake occurs at the initial time of the adsorption process due to unfilled adsorbent surface sites, effluent concentration becomes extremely low. The specific bed height where the adsorption takes place is known as the mass transfer zone (MTZ). After a time, the MTZ moves to the end of the fixed bed as the plug flow serves to increase effluent concentration. Finally, adsorbate concentration in the outlet solution is equal to that of the feed concentration. The area of the breakthrough curve presents the total amount of adsorbed metal ion.

This study presents kinetic adsorption models based on axial dispersion diffusion and pore diffusion resistances controlled by molecular diffusion mechanism. The pore size of nanostructured γ-alumina calculated according to the Barrett-Joyner-Halenda (BJH) method indicated that pore diameter was in the mesoporous range ($2 < d < 50$ nm) (Darezereshki *et al.* 2014) with a pore diameter of 4.6 nm. Knudsen diffusion is ignored due to having a small diameter of adsorbate molecule compared with the diameter of the adsorbent pores, and surface diffusion was ignored against pore diffusion because adsorbent pores have a large diameter. Rate variations and concentration gradient in the radial direction in the bed were ignored. Two parameters were applied to the equations; overall mass transfer coefficient ($K_{overall}$) and axial dispersion coefficient (D_z). Values for these parameters were obtained using the equations below.

A mathematical study of breakthrough analysis was performed using a one-dimensional model for isothermal, non-equilibrium, axially dispersed single component fixed-bed adsorption (Ghorai & Pant 2004). Partial mass balance for component i (the adsorbate) with selection of cylindrical

element from cylindrical bed is expressed as Equation (13) and definition of accumulation is based on Equation (14):

$$A\varepsilon\mu C - A\varepsilon D_z\frac{\partial C}{\partial z} = A\varepsilon\left[\mu C + \frac{\partial(\mu C)}{\partial z}\mu z\right] - A\varepsilon D_z\left[\frac{\partial C}{\partial z} + \frac{\partial^2 C}{\partial z^2}dz\right]\text{accumulation} \tag{13}$$

$$\text{accumulation} = \varepsilon \text{A} dz\frac{\partial c}{\partial t} + \varepsilon_p\frac{\partial c_p}{\partial t}(1-\varepsilon)adz + \rho_p\frac{\partial q}{\partial t}(1-\varepsilon)adz \tag{14}$$

In Equation (14), the first term is the accumulation of bulk fluid inside the element, the second term is moderate accumulation of fluid in the pores of the adsorbent inside the element, and the third term is moderate accumulation of the adsorbent inside the element. By rearranging Equations (13) and (14), the following is obtained:

$$-D_z\frac{\partial^2 C}{\partial z^2} + \frac{\partial(\mu C)}{\partial z} + \frac{\partial C}{\partial t} + \frac{1-\varepsilon}{\varepsilon}\left[\varepsilon_\text{p}\frac{\partial C_\text{p}}{\partial t} + \rho_\text{p}\frac{\partial q}{\partial t}\right] = 0 \tag{15}$$

N_i can be expressed using different formulas and various mass transfer resistances. The fluid phase driving force concentration was used for Equation (16) and the solid phase driving force was used for Equation (17) (Siahpoosh *et al.* 2009):

$$N_\text{i} = \frac{\partial C_\text{p}}{\partial t}\left(\varepsilon_\text{p} + \rho_\text{p}\frac{\partial q}{\partial C_\text{p}}\right) = k_\text{i}(C - C_\text{p}) \tag{16}$$

$$N_\text{i} = \rho_\text{p}\frac{\partial q}{\partial q} = k_\text{i}(q_\text{e} - q) \tag{17}$$

Equation (17) was used in the present study because the driving force of mass transfer is in the solid phase. The boundary and initial conditions are:

$$B.C.1\text{: } C(z,t) = C_o + \frac{Dz}{\mu}\frac{\partial C(z,t)}{\partial z},\ z = 0 \tag{18a}$$

$$B.C.2\text{: } \frac{\partial C(z,t)}{\partial z} = 0,\ z = l \tag{18b}$$

$$C\cdot(z,0) = 0 \tag{18c}$$

To calculate the overall mass transfer coefficient, both internal and external mass transfer resistances are added. The overall mass transfer coefficient is expressed as Equation (19) (Siahpoosh *et al.* 2009):

$$\frac{1}{K_\text{overall}} = \frac{R_\text{p}}{3k_\text{f}} + \frac{R_\text{p}^2}{15D_\text{p}^\text{e}\varepsilon_\text{p}} \tag{19}$$

The effective pore diffusivity coefficient, $D_\text{p}^{\,e}$ and D_p are calculated as Equations (20) and (21) (Yang 1987):

$$D_\text{p}^\text{e} = \frac{D_\text{p}}{\tau_\text{p}} \tag{20}$$

$$D_\text{p} = \frac{1}{\frac{1}{D_\text{m}} + (\frac{1}{D_\text{k}})} \tag{21}$$

Because of the small diameter of the adsorbate molecule compared with the adsorbent pore diameter, the Knudsen diffusion is ignored. Thus, Equations (20) and (21) are simplified as:

$$D_\text{p}^\text{e} = \frac{D_\text{m}}{\tau_\text{p}} \tag{22}$$

Since the path of molecule movement into the adsorbent pores is not direct, a tortuosity factor is calculated as Equation (23) (Wakao & Smith 1962):

$$\tau_\text{p} = \frac{1}{\varepsilon_\text{p}} \tag{23}$$

The Re and Sc values are in the range of experimental conditions, and there is agreement with Wakao and Funzakri; the mass transfer coefficient between the fluid and adsorbent particles is given by Equation (24) (Wakao & Funazkri 1978):

$$sh+ = \frac{k_\text{f}d_\text{p}}{D_\text{m}} = 2 + 1.1(Sc)^{0.33}(Re)^{0.6} \tag{24}$$

This relation is valid for $3 < \text{Re} < 10{,}000$ and $0.6 < \text{Sc} < 70$.

Since fluid velocity is low, axial dispersion is assumed for this packed bed. The axial dispersion coefficient is

calculated as Equation (25) (Wakao & Funazkri 1978):

$$\frac{D_z}{D_m} = \gamma_1 + \gamma_2 \frac{dpu}{D_m} = \gamma_1 + \gamma_2 \frac{(Re).(Sc)}{s} \quad (25)$$

where $\gamma_1 = 20/\varepsilon$ and $\gamma_2 = 0.5$. These values were selected because they provide the best empirical fit for the experimental results.

Effect of bed height

Figure 5 shows the breakthrough curve for metal ion adsorption at different bed heights of 5, 10 and 15 cm at a constant influent concentration (100 mg/L) and constant flow rate (6 mL/min). In this study, the breakthrough point occurred when effluent concentration reached 1% of the influent concentration. Moreover, bed saturation point occurred when effluent concentration reached 99% of influent concentration. Figure 5 shows that at bed heights of 5, 10 and 15 cm, breakthrough times of 90, 210 and 380 min were obtained and that bed saturation times were obtained at 888 minutes, 1857 minutes and 2737 minutes, respectively. The results showed that on increasing the bed height from 5 to 10 and to 15 cm, the saturation time increased by 109.1% and 208.2%, respectively. This result indicates that the slope of the breakthrough curve became more gentle according to the increased bed height; therefore, breakthrough and saturation times increased. At the different bed heights, 5, 10 and 15 cm, the adsorption capacities of the adsorbent were 38.62 mg/g, 42.6 mg/g and 44.99 mg/g, respectively. This result indicates that adsorption capacity of the adsorbent increased according to an increased bed height due to an increase in adsorbent active sites. In accordance with similar works, Ghorai & Pant (2004) evaluated fluoride adsorption by activated alumina in a fixed-bed column. These studies showed that a gentle slope of the breakthrough curve in relation to an increasing bed height from 5 to 10 cm and the MTZ became more extensive and saturation time increased.

Effect of flow rate

The effect of flow rate was studied at 3, 6 and 9 mL/min while the influent lead concentration and bed height were kept constant at 100 mg/L and 10 cm for all three experiments, respectively. Its characteristic curve is shown in Figure 6. At flow rates of 3, 6 and 9 mL/min, evaluations for adsorption capacity of the adsorbent were obtained at 47.79 mg/g, 42.6 mg/g and 38.15 mg/g, respectively. These results indicate that at lower flow rates, due to more non-saturated adsorption sites, the tendency for metal ion adsorption increases so that the adsorption process is more effective. At the different flow rates of 3, 6 and 9 mL/min, breakthrough times of 600, 210 and 115 minutes were obtained and saturation times of 3390 minutes, 1857 minutes and 1161 minutes were obtained, respectively. With increased flow rate of 3–6 and 9 mL/min, saturation time decreased by 45.2% and 65.7%, respectively. These values indicate that the metal ions had greater residence time on the adsorbent bed at lower flow rates.

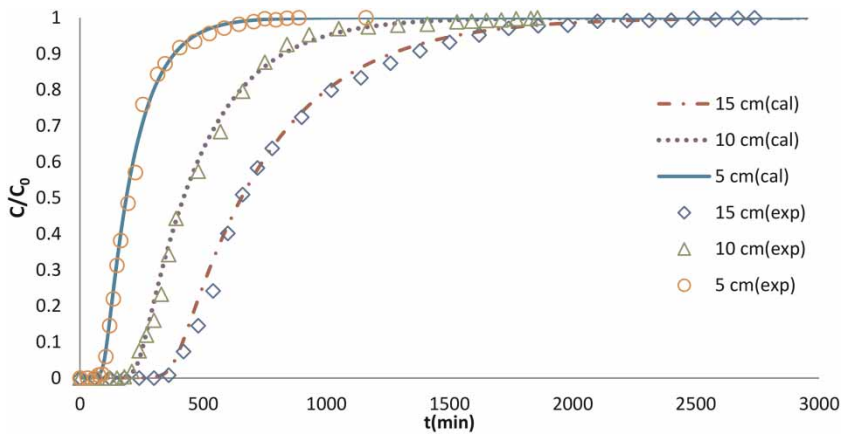

Figure 5 | Comparison of experimental breakthrough curves with different theoretical bed heights ($C_0 = 100$ mg/L, $Q_0 = 6$ mL/min).

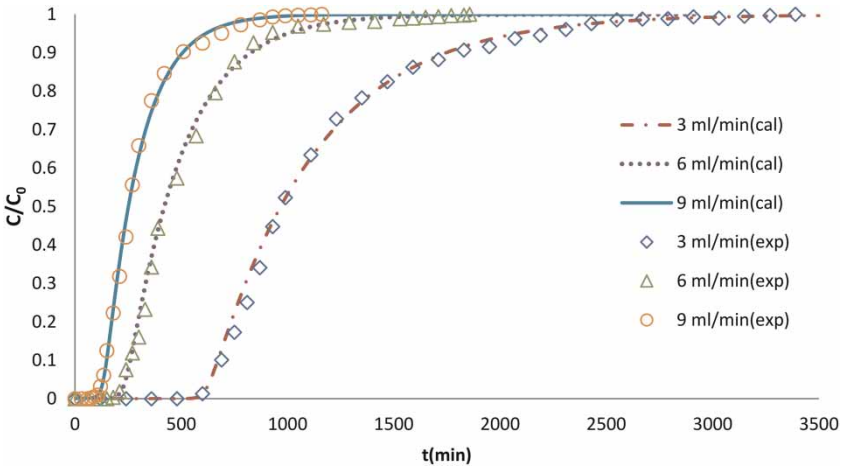

Figure 6 | Comparison of experimental breakthrough curves with different theoretical flow rates ($C_0 = 100$ mg/L, $L_0 = 10$ cm).

Effect of initial lead concentration

The column was tested with different initial lead concentrations of 65, 100 and 150 mg/L. The flow rate and bed height were kept at 6 mL/min and 10 cm, respectively (Figure 7). At the different aforementioned initial concentrations, breakthrough times were obtained at 300, 210 and 120 minutes and saturation time occurred after 2456 minutes, 1857 minutes and 1440 minutes, respectively. Under increasing initial concentrations of 65–100 and 150 ppm, saturation time decreased to 24.3% and 41.3%, respectively. Under decreased influent metal ion concentration, breakthrough time increased and there was a decrease of the slope of the breakthrough curve. At the different initial lead concentrations of 65, 100 and 150 mg/L adsorption capacity of adsorbent were obtained at 39.89 mg/g, 42.60 mg/g and 43.59 mg/g, respectively.

Comparisons were made between theoretical data obtained from equations (solid and dashed lines) and simultaneous solving with experimental data (individual points) obtained from experiments. The results are presented in Figures 5–7.

Model parameters under various operating conditions in the fixed-bed column, experimental and calculated maximum adsorption capacity and standard deviation values are listed in Table 2. Sensitivity of the model to the corresponding parameters (D_z, $K_{overall}$) was high and it was related to theoretical parameters of the model, not

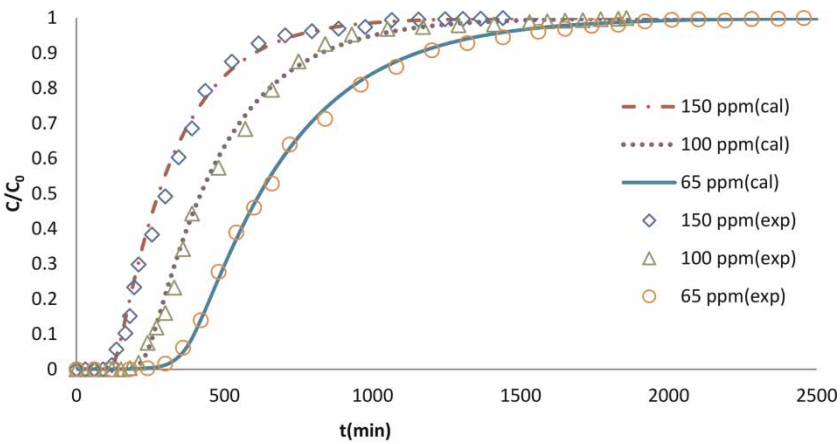

Figure 7 | Comparison of experimental breakthrough curves with different theoretical initial concentrations ($Q_0 = 6$ mL/min, $L_0 = 10$ cm).

Table 2 | Lumped model parameters in the fixed-bed column ($D_p^{e=7.5542\times10^{-10}}$ m^2/s)

Q (mL/min)	L (cm)	C_0 (mg/L)	$K_{overall}$ (1/s)	D_z (m^2/s)	$q_{max(exp)}$ (mg/g)	$q_{max(cal)}$ (mg/g)
3	10	100	3.51×10^{-5}	2.0621×10^{-6}	47.79 ± 0.04	47.12
9	10	100	1.08×10^{-4}	8.8251×10^{-5}	38.15 ± 0.03	37.89
6	10	100	6.77×10^{-5}	3.1321×10^{-5}	42.60 ± 0.01	41.91
6	5	100	1.41×10^{-4}	2.9287×10^{-5}	38.62 ± 0.04	37.95
6	15	100	4.51×10^{-5}	3.5416×10^{-5}	44.99 ± 0.02	43.31
6	10	65	5.28×10^{-5}	4.5856×10^{-5}	39.89 ± 0.02	39.22
6	10	150	8.42×10^{-5}	2.7138×10^{-5}	43.59 ± 0.05	42.93

operational parameters. They were given to four decimal digits. The results indicate that increasing flow rate and consequently increasing R_e served to increase D_z, as shown in Equation (25). The lead concentration gradient decreased as initial lead concentration increased, thus it can be concluded that D_z decreased. Overall, mass transfer resistance decreased as the flow rate increased, thus, $K_{overall}$ increased. $K_{overall}$ increased as the metal ion concentration increased and consequently, the concentration gradient decreased. According to Fick's law with constant mass transfer flux, $K_{overall}$ increased.

CONCLUSION

Studies on batch and continuous adsorption using nanostructured γ-alumina to remove Pb(II) indicated that this adsorbent had a high ability to remove heavy metal ions from aqueous solutions. In the batch study, the effect of various factors such as pH, initial solution concentration and contact time on Pb(II) adsorption onto nanostructured γ-alumina were investigated.

The results showed that removal efficiency (removal efficiency means removal percentage of adsorbate from aqueous solution or amount of adsorbate adsorbed on the adsorbent) increased with increasing contact time due to an increased contact of metal ions with the adsorbent. The adsorption reached its maximum efficiency after 150 minutes. The uptake of lead was negligible at a lower pH value and the amount of adsorption increased with increased pH value so that the maximum adsorption percentage was 92.71% at pH 4.5. The pH_{pzc} was 8.3 for nanostructured γ-Al_2O_3. With regards to the correlation coefficient (R^2) and the error functions (MPSD and chi-square) for Langmuir, Freundlich and Temkin isotherms, the Langmuir isotherm performed best in terms of adsorbent equilibrium behavior owing to a higher R^2 and the least number of errors, compared with the other two isotherms. The maximum adsorption capacity of adsorbent for Pb^{2+} was determined to be 119.04 mg/g. Considering the dimensionless constant of separation factor (R_L) between zero and one ($R_L = 0.16$), it can be interpreted that Pb(II) had favorable adsorption onto nanostructured γ-alumina. Adsorption capacity was also highly dependent on flow rate, influent lead concentration and bed height. Breakthrough and saturation times decreased at higher flow rates, lower bed heights and higher influent concentrations. The adsorption capacity of the adsorbent increased at lower flow rates, higher bed heights and higher influent concentrations. According to the changes in the slope of the adsorption capacity under various operating conditions, it can be concluded that the effect of the concentration was greater than that of bed height and that the effect of bed height was greater than that of flow rate on removal of Pb^{2+} from the aqueous solution.

The lumped method can predict Pb(II) adsorption onto nanostructured γ-Al_2O_3 through a bed under different operating conditions. The model includes the three mechanisms of pore diffusion, surface diffusion and axial dispersion diffusion.

Surface diffusion resistance was ignored because of its trace value. The theoretical breakthrough curve was drawn from the batch isotherm data and followed the pattern of the experimental breakthrough curve. Parameters applied to the model included overall mass transfer coefficient ($K_{overall}$) and axial dispersion coefficients (D_z); these were

obtained by fitting the experimental data to the theoretical model.

ACKNOWLEDGEMENTS

The authors wish to thank Mr Mohammad Kavand and Mr Esmaeel Darezereshki for their helpful support.

REFERENCES

Afkhami, A., Tehrani, M. S. & Bagheri, H. 2010 Simultaneous removal of heavy-metal ions in wastewater samples using nano-alumina modified with 2,4-dinitrophenylhydrazine. *J. Hazard. Mater.* **181**, 836–844.

Ahmedna, M., Marshall, W. E., Husseiny, A. A., Rao, R. M. & Goktepe, I. 2004 The use of nutshell carbons in drinking water filters for removal of trace metals. *Water. Res.* **38**, 1062–1068.

APHA, AWWA, WEF 2005 *Standard Methods for the Examination of Water and Wastewater*. American Public Health Association, Washington.

Barakat, M. A. 2011 New trends in removing heavy metals from industrial wastewater. *Arabian. J. Chem.* **4**, 361–377.

Bhatnagara, A., Kumarb, E. & Sillanpaac, M. 2010 Nitrate removal from water by nano-alumina: Characterization and sorption studies. *Chem. Eng. J.* **163**, 317–323.

Boulinguiez, B., Le Cloirec, P. & Wolbert, D. 2008 Revisiting the determination of Langmuir parameters application to tetrahydrothiophene adsorption onto activated carbon. *Langmuir.* **24**, 6420–6424.

Cai, S. & Sohlberg, K. 2003 Adsorption of alcohols on γ-alumina (1 1 0 C). *J. Mol. Catal. A Chem.* **193**, 157–164.

Dabrowski, A. 2001 Adsorption-from theory to practice. *Adv. Colloid Interf. Sci.* **93**, 135–224.

Darezereshki, E., Tavakoli, F., Bakhtiari, F., Behrad Vakylabad, A. & Ranjbar, M. 2014 Innovative impregnation process for production of γ-Fe2O3-activated carbon nanocomposite. *Mater. Sci. Semicond. Process.* **27**, 56–62.

Dastgheib, S. A. & Rockstraw, D. A. 2002 A model for the adsorption of single metal ion solutes in aqueous solution onto activated carbon produced from pecan shells. *Carbon* **40**, 843–851.

Do, D. D. 1998 *Adsorption Analysis: Equilibria and Kinetics*. Imperial College Press, London.

Elouear, Z., Bouzid, J., Boujelben, N., Feki, M., Jamoussi, F. & Montiel, A. 2008 Heavy metal removal from aqueous solutions by activated phosphate rock. *J. Hazard. Mater.* **156**, 412–420.

Ghorai, S. & Pant, K. K. 2004 Investigations on the column performance of fluoride adsorption by activated alumina in a fixed-bed. *Chem. Eng. J.* **98**, 165–173.

Ho, S., Porter, J. F. & Mckay, G. 2002 Equilibrium isotherm studies for the sorption of divalent metal ions onto peat: Copper, Nickel and lead single component system. *Water Air Soil Pollut.* **141**, 1–33.

Ho, Y. S., Chiu, W. T. & Chung, C. W. 2005 Regression analysis for the sorption isotherms of basic dyes on sugarcane dust. *Bioresource. Tech.* **96**, 1285–1291.

Iannibello, A. & Marengo, S. 1979 A study of the chemisorption of chromium (VI), molybdenum (VI) and tungsten (VI) onto γ-alumina. *Stud. Surf. Sci. Catal.* **3**, 65–76.

Kim, M. S. & Chung, J. G. 2002 Removal of copper (II) ion by kaolin in aqueous solutions. *Envir. Eng. Res.* **7**, 49–57.

Mobasherpour, I., Salahi, E. & Pazouki, M. 2011 Removal of divalent cadmium cations by means of synthetic nano crystallite hydroxyapatite. *Desalination* **266**, 142–148.

Ngomsik, A. F., Bee, A., Draye, M., Cote, G. & Cabuil, V. 2005 Magnetic nano- and microparticles for metal removal and environmental applications: a review. *C. R. Chim.* **8**, 963–970.

Rahmani, A., Zavvar Mousavi, H. & Fazli, M. 2010 Effect of nanostructure alumina on adsorption of heavy metals. *Desalination* **253**, 94–100.

Samadi, M. T., Saghi, M. H., Ghadiri, K., Hadi, M. & Beikmohammadi, M. 2010 Performance of simple nano zeolite Y and modified nano zeolite Y in phosphor removal from aqueous solutions. *Iranian J. Health. Environ.* **3**, 27–36.

Sharma, Y. C., Srivastava, V. & Mukherjee, A. K. 2010 Synthesis and application of nano-Al_2O_3 powder for the reclamation of hexavalent chromium from aqueous solutions. *J. Chem. Eng. Data.* **55**, 2390–2398.

Siahpoosh, M., Fatemi, S. & Vatani, A. 2009 Mathematical modeling of single and multi-component adsorption fixed beds to rigorously predict the mass transfer zone and breakthrough curves. *Iran. J. Chem. Chem. Eng.* **28**, 25–44.

Sulaymon, A. H., Abid, B. A. & Al-Najar, J. A. 2009 Removal of lead copper chromium and cobalt ions onto granular activated carbon in batch and fixed-bed adsorbers. *Chem. Eng. J.* **155**, 647–653.

Temkin, M. I. & Pyzhev, V. 1940 Kinetics of ammonia synthesis on promoted iron catalyst. *Acta Phys. Chim. USSR* **12**, 327–356.

Unuabonah, E. I., El-Khaiary, M. I. & Olu-Owolabi, B. I. 2012 Predicting the dynamics and performance of a polymer-clay based composite in a fixed bed system for the removal of lead (II) ion. *Chem. Eng. Res. Design.* **90**, 1105–1115.

Wakao, N. & Funazkri, T. 1978 Effect of fluid dispersion coefficients on particle-fluid mass transfer coefficients in packed bed. *Chem. Eng. Sci.* **33**, 1375–1384.

Wakao, N. & Smith, J. M. 1962 Diffusion in catalyst pellets. *Chem. Eng. Sci.* **17**, 825–834.

Yang, R. T. 1987 *Gas Separation by Adsorption Process*. Butterworth Stoneham, Boston.

Zhang, L., Huang, T., Zhang, M., Guo, X. & Yuan, Z. 2008 Studies on the capability and behavior of adsorption of thallium on nano-Al_2O_3. *J. Hazard. Mater.* **157**, 352–357.

First received 19 November 2014; accepted in revised form 28 January 2015. Available online 13 March 2015